LNF-89/037

A. Codino, C. Federico, C. Grimani, M. Menichelli, E. Rongoni, I. Salvatori,
P. Spillantini, G. Basini, F. Bongiorno, A. Morselli, M. Occhigrossi, M. Ricci

SIMULATION OF LOW-ENERGY ANTIPROTON INTERACTIONS IN A SAMPLING CALORIMETER

Estratto da: Nuovo Cimento 103B, n.3 319 (1989)

IL NUOVO CIMENTO VOL. 103 B, N. 3 Marzo 1989

LNF-037/89

Simulation of Low-Energy Antiproton Interactions in a Sampling Calorimeter.

A. CODINO, C. FEDERICO, C. GRIMANI, M. MENICHELLI
E. RONGONI and I. SALVATORI
I.N.F.N., Sezione di Perugia - Perugia, Italia

P. SPILLANTINI
I.N.F.N., Sezione di Firenze - Firenze, Italia

G. BASINI, F. BONGIORNO, A. MORSELLI(*), M. OCCHIGROSSI and M. RICCI
INFN - Laboratori Nazionali di Frascati - Frascati (Roma), Italia

(ricevuto il 22 Dicembre 1988)

Summary. — This paper describes the Monte Carlo program used for the simulation of antiproton interactions at intermediate energy inside a brass streamer-tube tracking calorimeter, to be used in a search for antimatter in cosmic rays, in the high atmosphere. The calorimeter is sensitive in the kinetic-energy range (100 ÷ 5000) MeV and the Monte Carlo is tuned in this energy interval both for proton and antiproton interactions. The detector geometry, which consists of a set of plane slabs, may be easily extended to other calorimeter structures.

PACS 07.90 – Other topics in specialized instrumentation.
PACS 29.40 – Radiation detectors.

1. – Introduction.

The importance of measuring the abundance of antiprotons in the cosmic rays is well known(1). We plan to perform a measurement of the $\bar{p}$ flux in the high

(*) CNR fellowship.
(1) S. A. STEPHENS and R. L. GOLDEN: *Astron. Astrophys.*, **202**, 1 (1988); S. A. STEHENS and R. L. GOLDEN: *Space Sci. Rev.*, **46**, 31 (1987).

atmosphere by detecting $\overline{p}$ annihilation vertices using a high granularity tracking calorimeter. The apparatus which will be carried by a balloon at the altitude of 45 km in the northern emisphere (Canada) is made of a magnetic spectrometer, t.o.f. counters, MWPCs and a tracking calorimeter (fig. 1) here

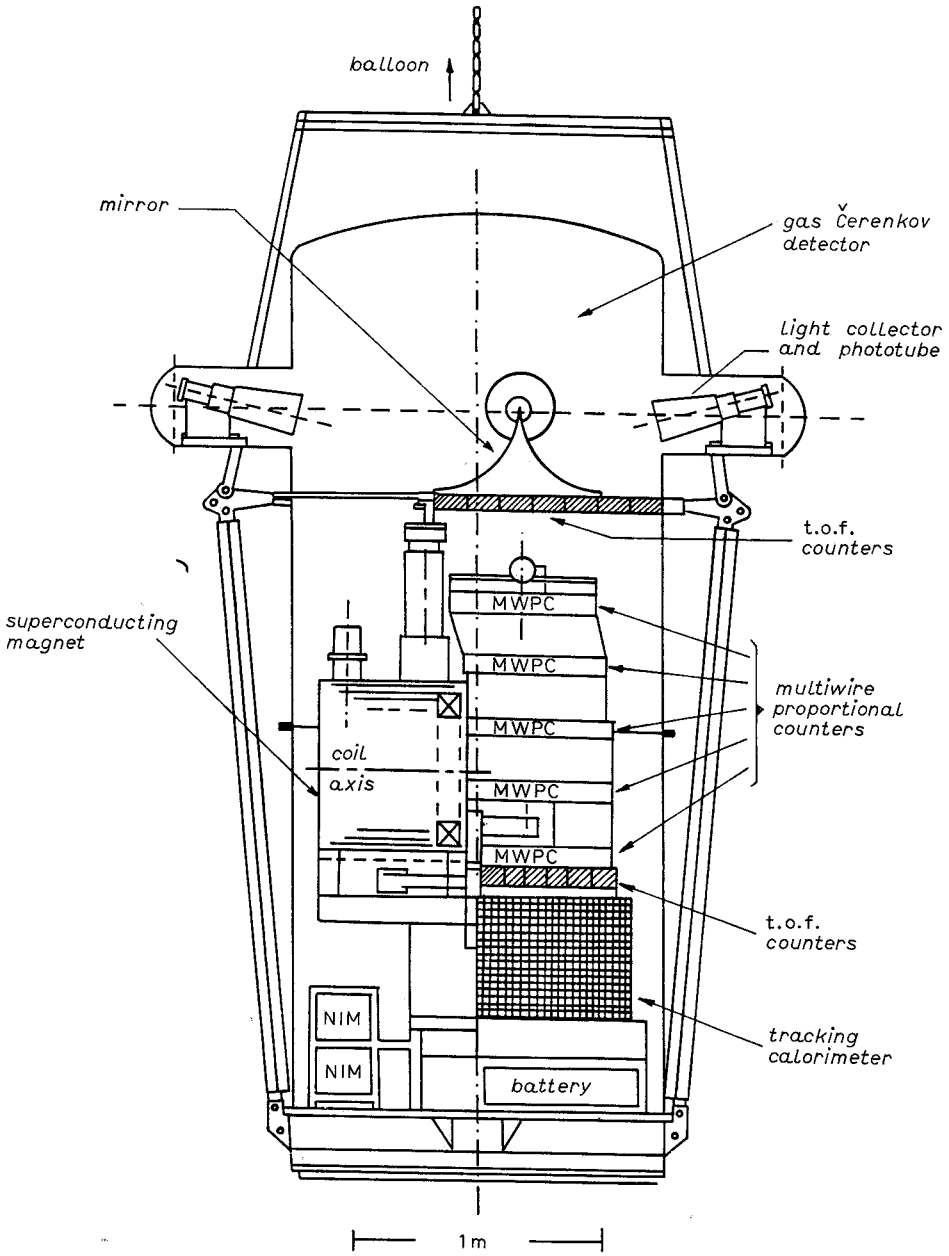

Fig. 1. – Layout of the balloon-borne apparatus for the detection of cosmic antiprotons.

described. The tracking calorimeter has been specifically designed and built for the identification of antiprotons by the annihilation pattern and by energy measurement in the range 100 MeV up to 5000 MeV.

In order to dispose of a computational tool comparable to the excellent calorimeter accuracy in resolving the annihilation vertices, we developed a simulation code for antiprotons interacting with the matter. Proton simulation was also performed to control the number of events induced by protons faking genuine $\overline{p}$ annihilation events.

The motivations for developing our Monte Carlo raise from the low-energy range useful to the experiment. In fact, existing, well-known simulation codes for hadronic interactions are specifically tuned for high-energy applications [2,3] where the approximations used are valid in that sector but inadequate for our experiment.

As an example, the number of secondaries produced in the hadron-nucleus interactions [2] is calculated by the KNO formula, while secondaries in our Monte Carlo are generated according to a parametrization of exclusive reactions for p-nucleon and $\overline{p}$-nucleon interactions. Another example of this inadequacy to low energies when simulating hadrons interacting with the matter [2,3] is the long itinerary from hadrons into quark structure functions and to quark fragmentation functions with the final reconversion of computed quantities into hadron measurable properties. Our program uses, at any step, hadrons and, as far as experimental data are available, only measured hadron properties.

This paper reports a preliminary description of the code and the first results obtained by the program applied to a specific detector.

2. – Geometry.

The gas calorimeter is a box of $(53 \times 53 \times 40)\,\text{cm}^3$ containing 50 planes of tubes operating in the streamer mode. Each tube of dimensions $(0.9 \times 0.7 \times 50)\,\text{cm}^3$ has a gold-plated tungsten wire (50 μm in diameter) supplied at about 4200 V.

One module is made of a brass frame constituting 8 tubes. A plane consists of 8 modules for a total of 64 tubes. Brass was chosen instead of more common plastic material because of the smaller geometrical cross-section ($(0.9 \times 0.7)\,\text{cm}^2$) yielding a better spatial resolution compared to plastic frames. The tracking capability has been enhanced by aluminium pick-up strips of dimensions $(0.01 \times 1 \times 50)\,\text{cm}^3$ glued on a vetronite (G10) support set at the opposite side to that of the brass modules. Strips run orthogonally to the wires to form a grid of rectangular coordinates for a total of 6400 independent read-out channels.

The model of this gas calorimeter considered by the simulation program is

---

[2] P. PAIGE and S. PROTOPOPESCU: ISAJET, BNL Report 31987 (1981).
[3] H. FESEFELDT: GHEISHA, PITHA Report 85/02 (1985).

shown in fig. 2. It consists of 200 rectangular layers of different materials such as brass, aluminium and G10 reaching 0.97 interaction lengths and 9.5 radiation lengths. The parameters of the calorimeter layers are reported in table I.

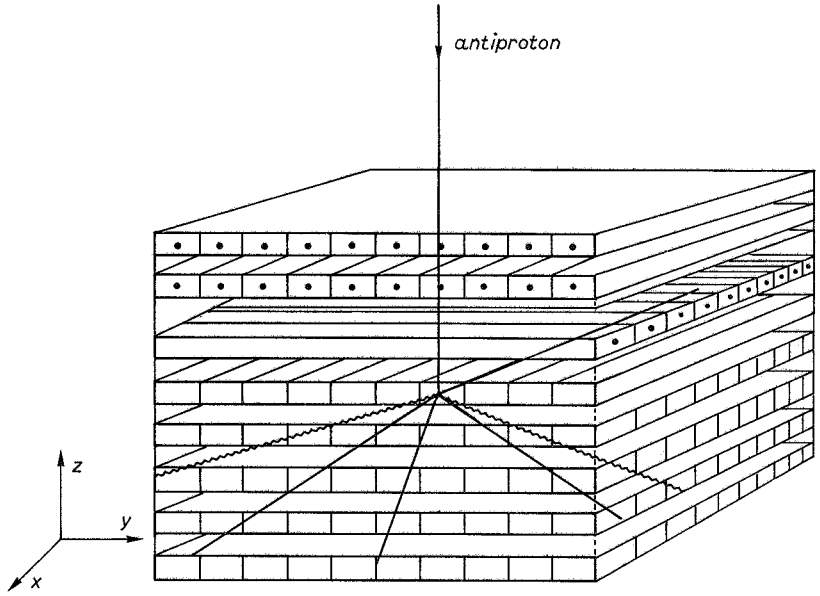

Fig. 2. – Model of the calorimeter formed of rectangular plates as is considered in the simulation program.

TABLE I. – *Main parameters defining the gas calorimeter in the simulation program.*

Tube material and density	Brass, 8.6 g/cm^3
Support material for strips and its density	G10, 1.7 g/cm^3
Brass composition	60% Cu, 40% Zn
G10 composition	60% SiO_2, 40% Epoxy; C_2OH_2
Thickness of a brass plane	0.275 cm
Thickness of a G10 plane	0.1 cm
Geometrical dimensions of the calorimeter	$(50 \times 50 \times 40)$ cm^3
Number of brass planes	47
Number G10 planes	47
Total thickness in interaction lengths	0.97
Total thickness in radiation lengths	9.5

3. – Transport of particles through the calorimeter.

As shown in fig. 2 the calorimeter in the Monte Carlo has been reduced to a set of rectangular slabs stacked in a box. The propagation of particles through the active and passive layers is accomplished by the following criteria:

1) The particle interaction probability is calculated for every brass or G10 slab.

2) The trajectory of charged particles is corrected for multiple scattering. Neutrons and antineutrons travel in straigth lines until they interact or leave the calorimeter.

3) Energy losses are calculated according to the Bethe Block formula with Sternheimer corrections [4]. For every layer of brass or G10, crossed by a particle, the propagation algorithm firstly checks if the particle interacts 1), then makes the corrections 2), 3) and finally calculates the intersection point with the next slab and repeats these iterations until the particle interacts or leaves the detector.

4) The electromagnetic showers, initiated by photons produced in π^0 decays, are simulated by another program [5] which takes into account the geometry of the calorimeter.

The penetration of particles through the stack of planar slabs as described in 3) may be tuned to satisfy the competing requests of saving computer time or achieving high accuracy in the parameters defining the transport of particle through the calorimeter layers. Note that, for computational purposes, the actual thickness of a layer can be replaced by a smaller thickness of more layers. If the layer thickness of this calorimeter (or any similar plane calorimeter) is kept thin, the algorithm for the evaluation of the cross-sections performs many iterations and the resulting accuracy may reach any desired level. Conversely, thick layers would save computer time degrading the accuracy in the transport simulation. This flexibility in choosing the larger thickness may result useful for charged pion interactions with matter because their cross-sections depend critically upon the pion momentum for low-energy interacting pions.

As the material of the layers is not a pure chemical element, the corresponding atomic weight A and the atomic number Z are taken by a suitable mixture of pure elements as described in ref. [6].

4. – Nuclear interactions.

The simulation of the interactions in the calorimeter takes place by two steps:

1) Calculation of the proton, antiproton and pion total cross-sections off nuclei and evaluation of whether or not the particle interacts.

---

[4] R. M. STERNHEIMER and R. F. PEIERLS: *Phys. Rev. B*, 3, 3681 (1971).
[5] A. CODINO: Thesis unpublished (1976). The program for simulation of electromagnetic showers in the matter is described in detail.
[6] PARTICLE DATA GROUP: REVIEW OF PARTICLES PROPERTIES: *Phys. Lett. B*, **170** (1986).

2) For those interactions occurring in the calorimeter, the number of secondaries are generated according to the relative probabilities of all possible final states which depend on the energy of the primary particle. These cross-sections are interpolation curves of available experimental data taken from ref. (7). Both the experimental data and the corresponding fits of several partial cross-sections are displayed in fig. 3. The simulation code has analogous fits of all

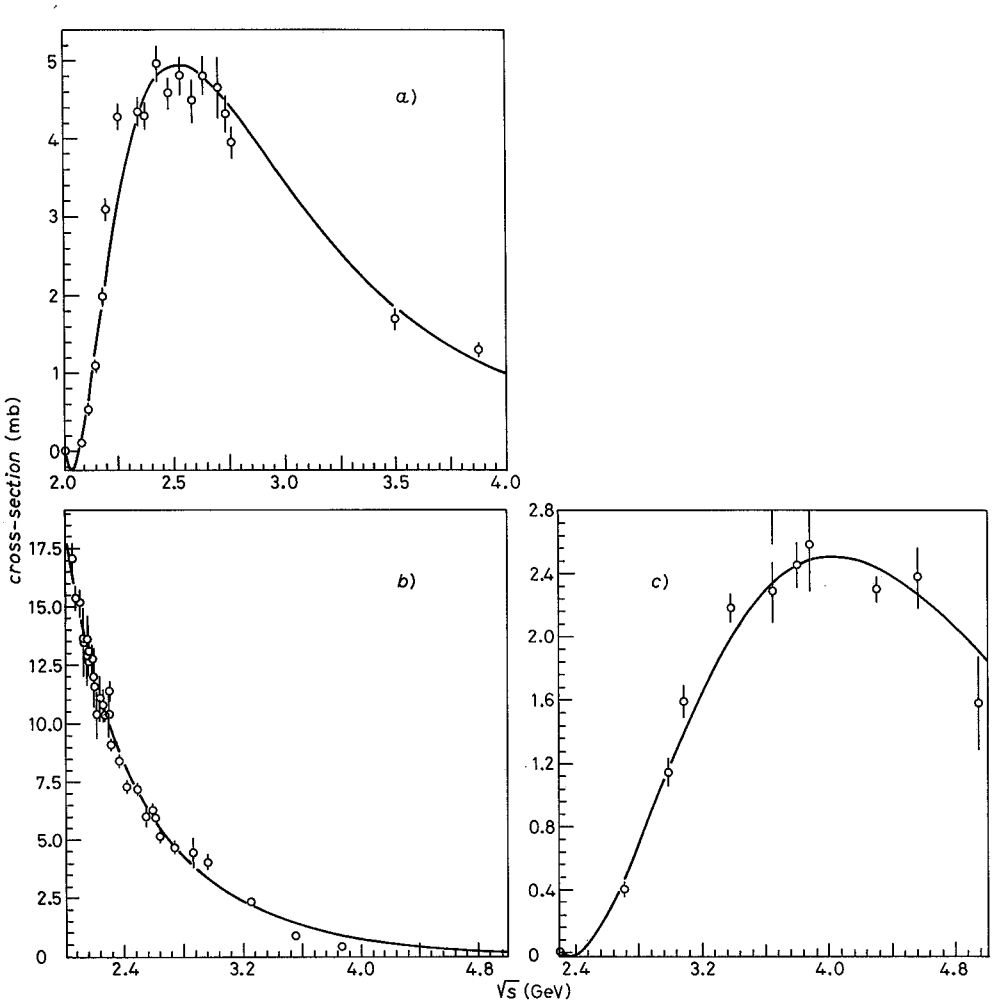

Fig. 3. – Fits of the experimental data for the cross-sections of the reactions *a)* $\overline{p}\,n \rightarrow$ $\rightarrow \overline{p}\,p\pi^-$, *b)* $\overline{p}\,p \rightarrow \pi^0 2\pi^- 2\pi^+$, *c)* $pp \rightarrow pn\pi^- 2\pi^+$. The program contains similar interpolation curves for all the reactions listed in table II.

(7) V. FLAMINIO, W. G. MOORHEAD, D. R. O. MORISON and N. RIVOIRE: *Compilation of cross-sections.* – III: p *and* $\overline{p}$ *induced reactions*, CERN-HERA Report 84-01 (April 1984).

TABLE II. – *Reactions concerning primary protons, antiprotons and charged pions presently included in the Monte Carlo.*

p + p interactions	p + n interactions
$p + p \to D + \pi^+$	$p + n \to p + n + \pi^+ + \pi^-$
$p + p \to p + n + \pi^+$	$p + n \to 2p + \pi^0 + \pi^-$
$p + p \to p + n + 2\pi^+ + \pi^-$	$p + n \to 2p + \pi^-$
$p + p \to p + p + \pi^+ + \pi^-$	$p + n \to p + n$
$p + p \to p + p + \pi^0 + \pi^+ + \pi^-$	
$p + p \to p + p + \pi^0$	
$p + p \to p + p$	
$\overline{p} + p$ interactions	$\overline{p} + n$ interactions
$\overline{p} + p \to n + \overline{n}$	$\overline{p} + n \to \pi^+ + 2\pi^-$
$\overline{p} + p \to \pi^+ + \pi^0 + \pi^-$	$\overline{p} + n \to \pi^+ + \pi^0 + 2\pi^-$
$\overline{p} + p \to p + \overline{p} + \pi^+ + \pi^-$	$\overline{p} + n \to p + \overline{p} + \pi^-$
$\overline{p} + p \to n + \overline{p} + \pi^+$	$\overline{p} + n \to 2\pi^+ + \pi^0 + 3\pi^-$
$\overline{p} + p \to p + \overline{p} + \pi^+ + \pi^- + \pi^0$	$\overline{p} + n \to 2\pi^+ + 3\pi^-$
$\overline{p} + p \to p + \overline{p} + \pi^0$	$\overline{p} + n \to n + \overline{p} + \pi^+ + \pi^-$
$\overline{p} + p \to 2\pi^+ + 2\pi^- + \pi^0$	$\overline{p} + n \to \pi^+ + 2\pi^0 + 2\pi^-$
$\overline{p} + p \to 2\pi^+ + 2\pi^-$	$\overline{p} + n \to \pi^+ + 3\pi^0 + 2\pi^-$
$\overline{p} + p \to p + \overline{n} + \pi^-$	$\overline{p} + n \to \pi^+ + 4\pi^0 + 2\pi^-$
$\overline{p} + p \to p^+ + \pi^- + 2\pi^0$	$\overline{p} + n \to \overline{p} + n$
$\overline{p} + p \to \pi^+ + \pi^- + 3\pi^0$	
$\overline{p} + p \to \pi^+ + \pi^- + 4\pi^0$	
$\overline{p} + p \to 2\pi^+ + 2\pi^0 + 2\pi^-$	
$\overline{p} + p \to 2\pi^+ + 3\pi^0 + 2\pi^-$	
$\overline{p} + p \to 2\pi^+ + 4\pi^0 + 2\pi^-$	
$\overline{p} + p \to 3\pi^+ + \pi^0 + 3\pi^-$	
$\overline{p} + p \to 3\pi^+ + 2\pi^0 + 3\pi^-$	
$\overline{p} + p \to 3\pi^+ + 3\pi^0 + 3\pi^-$	
$\overline{p} + p \to 2\pi^+ + 5\pi^0 + 2\pi^-$	
$\overline{p} + p \to \overline{p} + p$	
$\pi^+ + p$ interactions	$\pi^+ + n$ interactions
$\pi^+ + p \to \pi^+ + \pi^0 + p$	$\pi^+ + n \to p + \pi^0$
$\pi^+ + p \to 2\pi^+ + \pi^0 + \pi^- + p$	$\pi^+ + n \to p + \pi^+ + \pi^-$
$\pi^+ + p \to 2\pi^+ + \pi^- + p$	$\pi^+ + n \to p + 2\pi^0$
$\pi^+ + p \to n + 2\pi^+$	$\pi^+ + n \to \pi^+ + \pi^0 + \pi^- + p$
$\pi^+ + p \to \pi^+ + p$	$\pi^+ + n \to \pi^+ + n$
$\pi^- + p$ interactions	$\pi^- + n$ interactions
$\pi^- + p \to \pi^- + \pi^+ + n$	$\pi^- + n \to p + \pi^0 + 2\pi^-$
$\pi^- + p \to \pi^0 + n$	$\pi^- + n \to p + 2\pi^-$
$\pi^- + p \to \pi^0 + \pi^- + p$	$\pi^- + n \to \pi^- + n$
$\pi^- + p \to \pi^+ + 2\pi^- + p$	
$\pi^- + p \to n + 2\pi^0$	
$\pi^- + p \to 2\pi^- - \pi^+ + \pi^0 + p$	
$\pi^- + p \to \pi^- + p$	

reactions listed in table II. The interpolation curves have been calculated by the program MINUIT ([8]).

Note that the incident hadrons interact with a single nucleon because in our energy range it is $\lambda \ll R$, where λ is the wavelength of the incoming hadron and R is the nuclear radius.

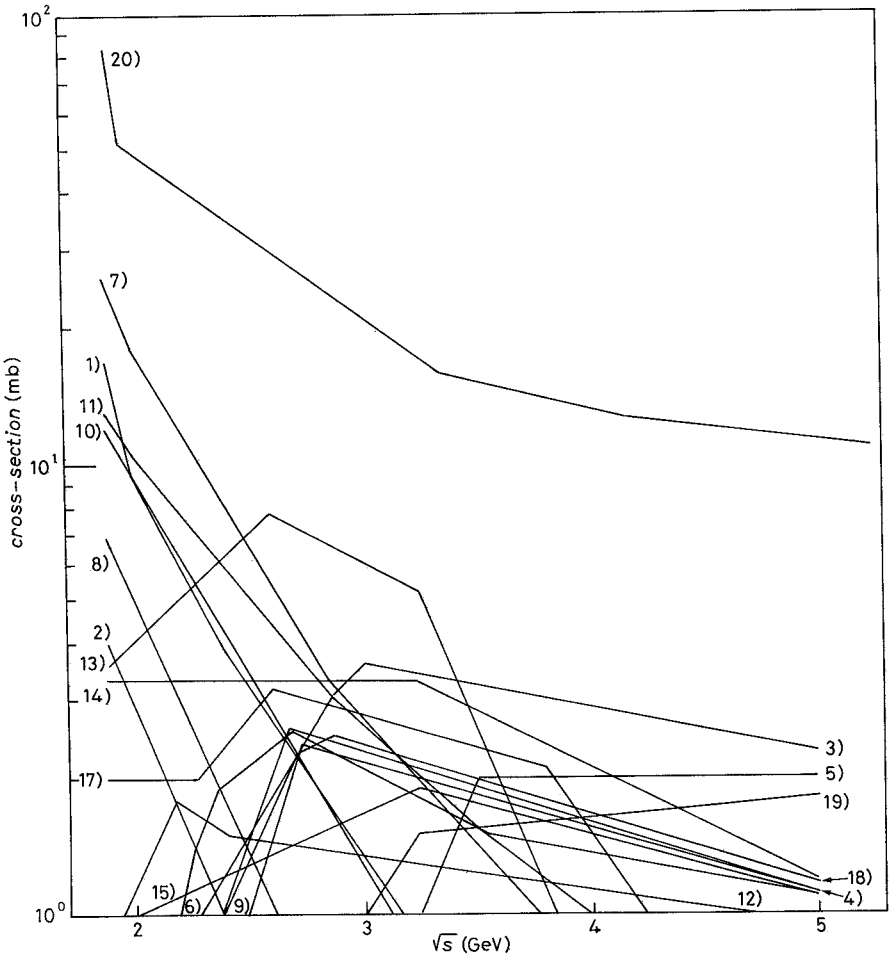

Fig. 4*a*. – Antiproton-proton partial cross-sections *vs.* total energy $\sqrt{s}$ considered in the simulation program. 1) $p\bar{p} \to n\bar{n}$, 2) $p\bar{p} \to \pi^+\pi^0\pi^-$, 3) $p\bar{p} \to p\bar{p}\pi^+\pi^-$, 4) $p\bar{p} \to n\bar{p}\pi^+$, 5) $p\bar{p} \to p\bar{p}\pi^+\pi^-\pi^0$, 6) $p\bar{p} \to p\bar{p}\pi^0$, 7) $p\bar{p} \to 2\pi^+2\pi^-\pi^0$, 8) $p\bar{p} \to 2\pi^+2\pi^-$, 9) $p\bar{p} \to p\bar{n}\pi^-$, 10) $p\bar{p} \to \pi^+\pi^-2\pi^0$, 11) $p\bar{p} \to \pi^+\pi^-3\pi^0$, 12) $p\bar{p} \to \pi^+\pi^-4\pi^0$, 13) $p\bar{p} \to 2\pi^+2\pi^-2\pi^0$, 14) $p\bar{p} \to$ $\to 2\pi^+2\pi^-3\pi^0$, 15) $p\bar{p} \to 2\pi^+2\pi^-4\pi^0$, 16) $p\bar{p} \to 2\pi^+2\pi^-5\pi^0$, 17) $p\bar{p} \to 3\pi^+3\pi^-\pi^0$, 18) $p\bar{p} \to$ $\to 3\pi^+3\pi^-2\pi^0$, 19) $p\bar{p} \to 3\pi^+3\pi^-3\pi^0$, 20) $p\bar{p} \to p\bar{p}$.

([8]) F. JAMES and M. ROOS: *Minuit. Minimization and error analysis*, CERN Program Library (1986).

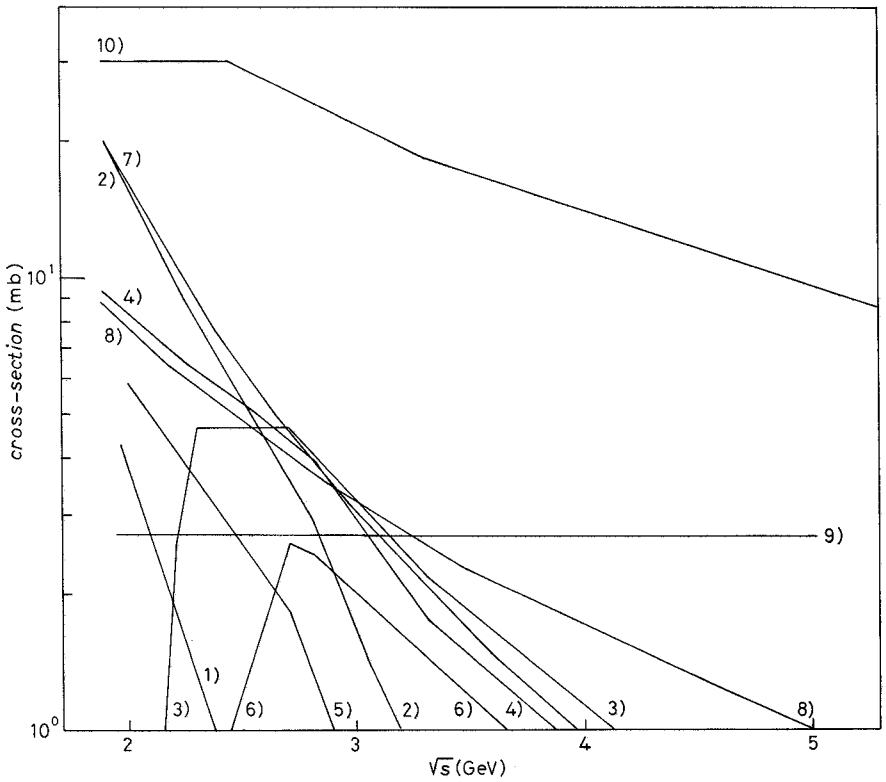

Fig. 4*b*. – Antiproton-neutron partial cross-sections *vs.* total energy $\sqrt{s}$. 1) $\overline{p}n \to \pi^+ 2\pi^-$, 2) $\overline{p}n \to \pi^+\pi^0 2\pi^-$, 3) $\overline{p}n \to p\overline{p}\pi^-$, 4) $\overline{p}n \to 2\pi^+\pi^0 3\pi^-$, 5) $\overline{p}n \to 2\pi^+ 3\pi^-$, 6) $\overline{p}n \to n\overline{p}\pi^+\pi^-$, 7) $\overline{p}n \to \pi^+ 2\pi^0 2\pi^-$, 8) $\overline{p}n \to \pi^+ 3\pi^0 2\pi^-$, 9) $\overline{p}n \to \pi^+ 4\pi^0 2\pi^-$, 10) $\overline{p}n \to \overline{p}n$.

The following approximations are also considered:

a) Due to the shadowing effect, the total cross-sections σ_T for hadrons interating with nucleus are not taken as the sum of the hadron-nucleon total cross-sections; we set

$$\sigma_T = A^\alpha \cdot \sigma ,$$

where $\alpha = 0.77$ according to ref. (6) and A is the atomic weight.

b) Neutron-proton total cross-section is parametrized from experimental data (7).

c) The nucleon momenta are distributed according to the Fermi model.

d) In those interactions where $\overline{p}$ annihilation does not occur, the target nucleon cannot leave the nucleus if the kinetic energy is below the nuclear binding energy. The resulting nuclear excitation energy is neglected.

Figure 4 shows the partial cross-sections as a function of total energy $\sqrt{s}$ for nucleon-nucleon interactions reported in table II and used in the Monte Carlo.

For interacting neutrons and antineutrons the available experimental data are not sufficient to give a complete parametrization of the partial cross-sections as those for protons and antiprotons. Therefore they are approximated as follows:

I) $\sigma(\mathrm{n}, \mathrm{n})$ as $\sigma(\mathrm{p}, \mathrm{p})$;
II) $\sigma(\overline{\mathrm{n}}, \mathrm{p})$ as $\sigma(\overline{\mathrm{p}}, \mathrm{n})$;
III) $\sigma(\overline{\mathrm{n}}, \mathrm{n})$ as $\sigma(\overline{\mathrm{p}}, \mathrm{p})$.

5. – Production of secondaries.

The generation of secondaries is performed by parametrizing ref. ([7]) the partial cross-sections for the reactions given in table II. These partial cross-sections are then normalized on the total cross-section.

The momenta of the products are calculated by a phase space momenta distribution generator which is available in the CERN Library, called GENBOD ([9]). This calculation uses the Raubold and Linch method to generate the momenta of the secondaries. The method is based on a recurrence relation derived from the original phase space integral that calculates momenta distribution by applying recursively the two-body phase space factor.

All partial cross-sections for neutrons and antineutrons interacting with nuclei are calculated with the approximations made for total cross-sections mentioned in the previous section.

6. – Results.

In this section we report the results obtained by the present version of the Monte Carlo for some useful parameters of the calorimeter which are relevant to our experiment.

In fig. 5 we show the neutral and charged pion multiplicity as a function of the incoming $\overline{\mathrm{p}}$ kinetic energy for annihilations taking place in the calorimeter. The higher multiplicity π^- with respect to that of π^+ is due to the large cross-section of the reaction $\overline{\mathrm{p}}\,\mathrm{n} \rightarrow \overline{\mathrm{p}}\,\mathrm{p}\,\pi^-$ which has no analogous channel producing π^+ in the ordinary matter. The computed multiplicity refers to the total number of pions which includes those of the $\overline{\mathrm{p}}$ annihilation and those eventually produced by

([9]) F. JAMES: *FOWL. General Monte Carlo phase space*, CERN Program Library (1986).

secondary nucleons and pions interacting in the calorimeter. Figure 5 also shows the average total energy for $\pi^0, \pi^-\pi^+$ emerging from the same annihilation events.

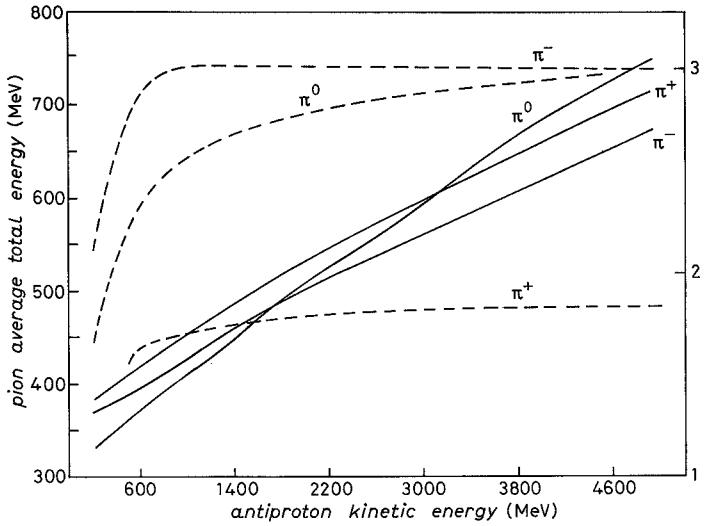

Fig. 5. – Pion multiplicities for $\overline{p}$ annihilation in the calorimeter. The average pion energy is also shown for the same events. —— total energy, --- multiplicities.

In fig. 6 is reported in detail that part of the apparatus (face of the calorimeter and the lowest lying MWPC as seen in fig. 1) which is capable of detecting particles scattered in the backward direction with respect to the nominal incident antiproton direction. The number of backward scattered particles depends critically on the distance d between the face of the calorimeter and the MWPC plane.

Figure 7 shows the average number of particles backward scattered per annihilation event (albedo) occurring in the calorimeter. Such calculations have been performed by varying the distance d for several $\overline{p}$ incident angles and for antiproton kinetic energies 500, 1000 and 1500 MeV. We assumed that any particle emerging from the $\overline{p}$ annihilation vertices is detected by the MWPC with full efficiency if the trajectory hits the chamber volume. Note also that the effect of the magnetic field on particle trajectories has been neglected in this calculation. The albedo is important in our experiment because backward scattered particles inhibit the acquisition trigger affecting the absolute $\overline{p}$ flux measurement.

Our present simulation code for $\overline{p}$ and p interactions consists of 16000 statements and takes, on the average, about 1.15 s of CPU time on the VAX 8650 to process one annihilation event.

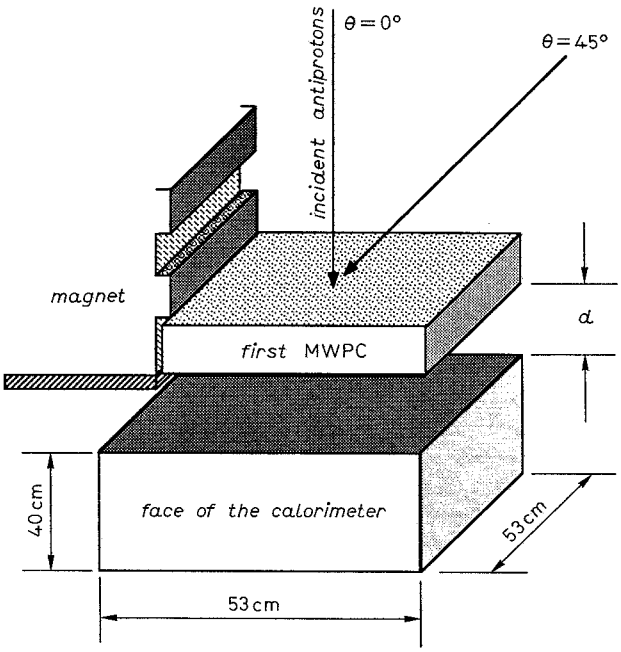

Fig. 6. – Layout of the front face of the calorimeter and the MWPC of the tracking system of the superconducting spectrometer.

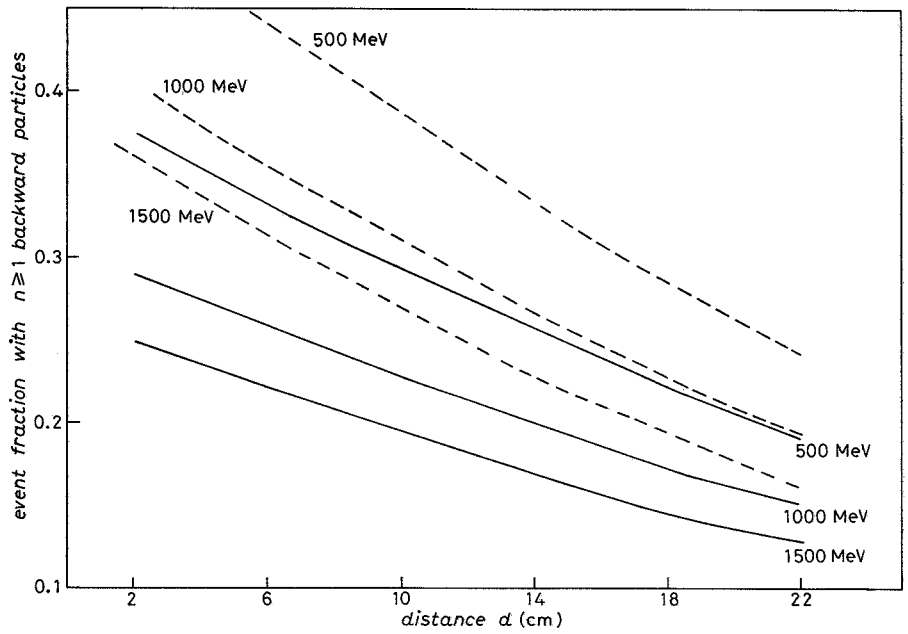

Fig. 7. – Event fractions with one or more than one pion scattered in the backward direction hitting the multiwire proportional chamber. —— $\theta = 0°$, ---- $\theta = 45°$.

We intend to upgrade our simulation code by I) including additional interaction channels especially those producing kaons, II) performing the simulation of secondary kaon interaction in the matter with the same accuracy as for $\pi^{\pm}$ and nucleons, III) implementing existing algorithms by more powerful sampling techniques to save computer time.

● RIASSUNTO

Questo articolo descrive il programma Monte Carlo utilizzato per la simulazione di interazioni di antiprotoni ad energia intermedia all'interno di un calorimetro tracciante a tubi a streamer in ottone, da impiegare nella ricerca in alta atmosfera di antimateria nei raggi cosmici. Il calorimetro è sensibile nell'intervallo di energie cinetiche ($100 \div 5000$) MeV ed il Monte Carlo è utilizzato in tale intervallo di energie sia per interazioni di protoni che di antiprotoni. La geometria del rivelatore, che consiste in una serie di piani sovrapposti, può essere estesa in modo semplice a calorimetri diversamente strutturati.

Моделирование взаимодействий антипротонов низких энергий в калориметре.

Резюме (*). — В этой статье описывается программа Монте-Карло для моделирования взаимодействия антипротонов промежуточных энергий внутри трекового калориметра, чтобы использовать его для поиска антивещества в космических лучах в верхних слоях атмосферы. Калориметр является чувствительным в области кинетических энергий от 100 МэВ до 5000 МэВ и программа Монте-Карло настроена на указанный энергетический интервал для взаимодействий протонов и антипротонов. Геометрия детектора, который состоит из системы плоскопараллельных пластин, может быть обобщена на случай других структур.

(*) *Переведено редакцией.*